Hybrid Power Flow Controller Steady-state Modeling, Control, and Practical Application

Behnam Tamimi, *Student Member, IEEE,* Claudio Cañizares, *Fellow, IEEE,* and Claudia Battistelli, *Member, IEEE*

***Abstract*—Steady-state models of the Hybrid Power Flow Controller (HPFC) for power flow and optimal power flow (OPF) studies are presented in this paper, considering the multiple control modes of the device. A strategy for control mode switching and limit handling in power flow calculations is proposed. The OPF model of the HPFC represents all the device control and physical limits as constraints in the mathematical formulation, so that the HPFC can be optimally dispatched as a part of the transmission system control assets. The power flow model is demonstrated and validated through loadability studies on a two-area benchmark test system, where the OPF model is used to determine the optimal ratings of the device based on a cost-benefit analysis. A study is also presented of the HPFC application to Ontario-Canada's grid, to address particular congestion problems in this network; an HPFC cost analysis is also shown for this system. The presented studies demonstrate the application of the proposed models for planning and operation studies, illustrating the performance, effectiveness, and feasibility of the controller to solve congestion issues in a real grid.**

***Index Terms*—Congestion relief, FACTS, HPFC, modeling, OPF, power flow.**

I. Introduction

FLEXIBLE AC Transmission System (FACTS) controllers offer new opportunities to better control power systems, as well as enhance power transfer capabilities [1]. Several Voltage-Source Converter (VSC) FACTS have been proposed in the literature, particularly the Static Synchronous Compensator (STATCOM), the Series Static Synchronous Compensator (SSSC), and the Unified Power Flow Controller (UPFC) [2]. Among these controllers, the UPFC is a versatile device that can control various system variables independently [3] (e.g. bus voltage magnitudes and transmission line active and reactive power flows), and its application to solve congestion problems in an actual grid is demonstrated in [4]. However, the capital cost of this controller is a major obstacle for the wide application of this technology in power systems. Thus, a cost effective VSC-based FACTS controller is introduced in [5], which yields operating characteristics similar to those of the UPFC while requiring a lower capital investment. This controller may consist of converters as well as passive components (e.g. capacitor banks), and is referred to as the Hybrid Power Flow Controller (HPFC). Compared to the UPFC, the savings stem from a few structural differences between the two devices, including the use of half-sized converters and passive elements for supplying the bulk of the required reactive power, as discussed in [5].

The benefits of an HPFC are defined by its limits and operating constraints. Therefore, the impact of the controller limits on its performance must be considered during planning and operation stages. However, previously published works on the HPFC do not discuss the device operating limits and their implications in congestion studies adequately [5]–[7]. Thus, in [5], the device is introduced, and an interesting geometrical representation of the devices operating region is presented. An Electromagnetic Transients Program (EMTP) model of the HPFC is briefly studied in [6]. The performance of the HPFC with regard to improving the power transfer capability of a system is compared with that of the UPFC in [7], based on time domain simulations.

In the current paper, a novel model of the HPFC appropriate for congestion studies, which are for the most part based on power-flow analyses, and its various possible control modes are presented and applied to address congestion issues. The controller is modeled from the system point of view, and thus its terminals are considered in the model, which is consistent with its operation requirements. The controller's internal variables are also properly represented in the proposed model, which allows handling the device limits accurately and thus modeling the multiple control modes defined in this paper. The proposed model is integrated into a widely popular power flow production program using a sequential approach to allow its integration into commercial power system analysis software packages. An HPFC model for OPF applications is also introduced, proposing a concise mathematical model of the HPFC for OPF applications that considers the device ratings and its control variables and limits directly. These proposed models are then used to demonstrate their applications in planning and operation studies, evaluating the performance and the effectiveness of the device using realistic test systems and practical assumptions and scenarios.

The rest of the paper is organized as follows: After reviewing the basics of the HPFC in Section II, its steady-state circuit model and associated operating modes are introduced in Section III, together with an effective strategy to handle the operating limits in power flow studies. The device model for OPF applications is presented in Section IV. In Section V, the device is applied to address congestion issues in two test systems, namely, a two-area system and a detailed model of Ontario-Canada's grid; several studies based on the proposed model and realistic scenarios are carried out to evaluate the performance and show the benefits of the HPFC, demonstrating the feasibility of the device to solve actual congestion

This work has been supported by NSERC and Hydro One Inc. through a Collaborative Research and Development (CRD) grant.

B. Tamimi, C. Cañizares are with the Department of Electrical and Computer Engineering, University of Waterloo, Waterloo, ON, Canada (e-mail: ccanizares@uwaterloo.ca).

C. Battistelli is currently with the Department of Electrical and Electronic Engineering, Imperial College, London, UK (e-mail: c.battistelli@imperial.ac.uk).

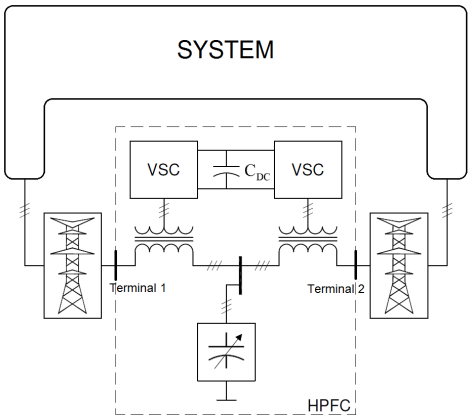

Fig. 1. The HPFC Architecture.

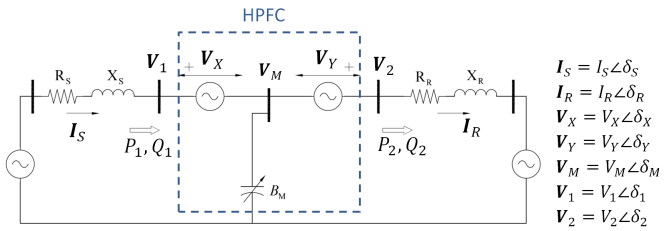

Fig. 2. Circuit model for the HPFC in a system.

problems in real networks. Finally, Section VI summarizes the paper's conclusions and contributions.

II. HPFC Review

The architecture of a typical HPFC is shown in Fig. 1 [5], with the core of the controller being a variable shunt susceptance accompanied by two converters and their transformers. In this figure, the shunt device can be a Static VAr Compensator (SVC) or a passive (switchable) capacitor bank, and the converters share a common dc link to exchange active power; if the active power loss inside the device is ignored, its net exchange of active power with the system is zero. The converter outputs as well as the shunt susceptance are changed to regulate the power flow through the associated line, and consequently the power exchange between the two line terminals. If there is another corridor between the two line terminals, parallel to the one with the HPFC, the power flow through that corridor can be controlled indirectly using this device. The controller can also be used to regulate its terminal voltages. Power and voltage regulation is feasible as long as the device stays within its capability limits.

Figure 2 shows the circuit model for the HPFC as seen from system's point of view. A variable shunt susceptance with two series voltage sources represent the main components of the controller. Voltage phasors $\boldsymbol{V}_1$ and $\boldsymbol{V}_2$ represent the controller terminals (1 and 2), which are connected to the system represented by its Thevenin equivalents at the controller terminals; the leakage reactances of the controller series transformers are included in the equivalent Thevenin impedances.

The HPFC has four possible control modes which are defined here as PVV, PQQ, V, and Z. The topology of the controller is the same in PVV and PQQ modes, which is not the case in other modes. In the PVV mode, setpoints for P, V_1, and V_2 values are defined, while in the PQQ mode, the values for P, Q_1, and Q_2 are set. It is important to note that when the controller limits are reached in the PQQ mode, the values of P, Q_1, and Q_2 are obtained by the limit handling strategy proposed here and are not known beforehand. In the V mode, the powers cannot be regulated because of the controller limits being reached, with the controller turning into a shunt voltage regulator with the two series voltage sources bypassed; the voltage setpoint in the V mode can be assumed to be the same as a terminal voltage value in the PVV mode, with the voltage regulation being achieved by changing the variable shunt susceptance. This shunt susceptance may reach its limit at certain power transfer level; therefore, the controller at that point is seen by the network as a fixed value, which is referred here as the Z mode. Note that in V and Z modes, $V_1 = V_2 = V_M$ and $V_X = V_Y = 0$.

III. HPFC Modeling

The main operating limits of the controller are considered on the following variables and parameters, defined in Fig. 2:

- The device main currents: I_S and I_R.
- Inverter voltages: V_X and V_Y.
- Shunt device voltage and susceptance: V_M and B_M.

In practical cases, the maximum allowable values for V_X and V_Y is small (e.g. 0.05 p.u.), to keep the inverter rating and cost as low as possible. Thus, the limit for $V_M = |\boldsymbol{V}_M| = |\boldsymbol{V}_1 - \boldsymbol{V}_X| = |\boldsymbol{V}_2 - \boldsymbol{V}_Y|$ is dependent on the terminal voltages $\boldsymbol{V}_1$ and $\boldsymbol{V}_2$. Note that the currents flowing through the series branches ($\boldsymbol{I}_S$ and $\boldsymbol{I}_R$) and their magnitude limits are represented and handled directly, which improves the numerical stability of the model [1]. The control limit handling strategy for I_S, I_R, V_X, V_Y and B_M is explained next.

The default control mode for the HPFC is defined here as PVV, in which the active power flow and the voltage magnitudes at the controller terminals are independently controlled. However, based on the system conditions and the controller operating limits, the HPFC may switch to other control modes. The controller operating constraints are increasingly relaxed as it moves from PVV to the other previously defined control modes, i.e. PQQ, V, and finally Z control modes.

The transitions between the four control modes defined here are shown in Fig. 3. The controller starts operating in the PVV mode, where setpoints for P, V_1, and V_2 are defined. If the controller reaches its limits on at least one of the main variables, i.e. I_S, I_R, V_X, or V_Y, the controller switches to PQQ mode, in which setpoints for P, Q_1, and Q_2 are defined to resolve the limit violation, so that these values are close to those corresponding to the PVV mode; these values are obtained using the linearization approach explained in Section III-B. The HPFC continues operating in the PQQ mode until the limit violations cannot be resolved by the modification of the P, Q_1, and Q_2 setpoints, at which point the controller switches to V mode.

In the V mode, the two series voltage sources in Fig. 2 are bypassed, and the voltage magnitude at the shunt bus

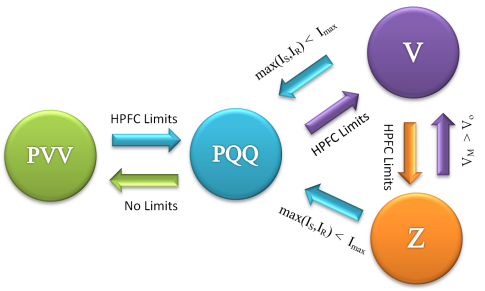

Fig. 3. Transitions between the four defined HPFC control modes.

V_M is regulated at a given level by using the variable shunt susceptance B_M; in this mode, $V_1 = V_2 = V_M$, so that the terminal voltages are regulated as well. This voltage regulation is feasible as long as the shunt device is capable of providing the required B_M value, but this is not always possible because of its limited capability, at which point B_M is fixed and the controller switches to Z mode. In this mode, the controller has its minimum regulation capability and behaves as a passive fixed shunt susceptance in the system.

The path from the PVV mode through PQQ, V, and Z modes can be associated with a gradual increase in the HPFC loading. In this case, the device responds to the higher demand by relaxing more operating constraints to avoid exceeding the device ratings. However, recovery is also possible when the loading level decreases, and stricter regulation becomes feasible. The control mode switching logic is explained in detail next.

A. PVV Mode (Default Mode)

In this mode, the controller is assumed to regulate the active power flow and the terminal voltages at a given level; this is feasible as long as the controller stays within its capability limits. In the case of a limit violation that is not relieved by changing the B_M value (see Section III-B3), the controller is assumed to switch to the previously described PQQ mode, and the internal voltages and currents are modified to bring the controller within its limits. In the case of a non-convergent power flow, the control mode is switched to V mode, which is a conservative approach that considers all possible scenarios before declaring a true non-convergent power flow.

B. PQQ Mode

The proposed strategy for the PQQ mode tries to keep currents and voltages at the same time away from their limits. The approach is based on the sensitivity of the controller power injections with respect to its internal voltage and current magnitudes, as explained in Section III-B1. In this strategy, B_M can be considered to be a discrete parameter. The flowchart of the proposed strategy is shown in Fig. 4, with the internal voltages and currents being modified to bring the controller within its limits; this is accomplished using the sensitivity analysis explained next. It is critical to start with a reasonable value for the shunt device susceptance B_M; thus, a proper value should be choosen first, as discussed in Section III-B3.

New values for P, Q_1, and Q_2 are calculated using a sensitivity matrix G and the magnitude of the limit violation. These new values are used to run a power flow, which if it converges, the results are checked for any limit violation; otherwise, the incremental step is halved, as explained in Section III-B1, and the power flow analysis is repeated. This procedure is iterated a few times (e.g. $m_{max} = 2$) until convergence is achieved; limit violations are also checked iteratively a few times (e.g. $n_{max} = 2$). In either of these loops, if the maximum iteration number is reached without achieving convergence or resolving the limit violation, the control mode is switched to V mode to relax power regulation; otherwise, the final results are displayed.

1) PQQ Setpoint Calculation: The desired P, Q_1, and Q_2 values and the sensitivity matrix G are determined as follows: From Fig. 2, P, Q_1, and Q_2 can be readily obtained; therefore, their derivatives can be derived, assuming that the devices terminal voltages are stiff, resulting in the following matrix G:

$$G = \begin{bmatrix} \frac{\partial P}{\partial I_S} & \frac{\partial P}{\partial I_R} & \frac{\partial P}{\partial V_X} & \frac{\partial P}{\partial V_Y} \\ \frac{\partial Q_1}{\partial I_S} & \frac{\partial Q_1}{\partial I_R} & \frac{\partial Q_1}{\partial V_X} & \frac{\partial Q_1}{\partial V_Y} \\ \frac{\partial Q_2}{\partial I_S} & \frac{\partial Q_2}{\partial I_R} & \frac{\partial Q_2}{\partial V_X} & \frac{\partial Q_2}{\partial V_Y} \end{bmatrix} \tag{1}$$

The power changes can then be calculated as follows:

$$\begin{bmatrix} \Delta P \\ \Delta Q_1 \\ \Delta Q_2 \end{bmatrix} = k^m G \begin{bmatrix} \min\left(0, (I_{Smax} - I_{So})\right) \\ \min\left(0, (I_{Rmax} - I_{Ro})\right) \\ \min\left(0, (V_{Xmax} - V_{Xo})\right) \\ \min\left(0, (V_{Ymax} - V_{Yo})\right) \end{bmatrix} \tag{2}$$

$$\begin{bmatrix} P \\ Q_1 \\ Q_2 \end{bmatrix} = \begin{bmatrix} P_o \\ Q_{1o} \\ Q_{2o} \end{bmatrix} + \begin{bmatrix} \Delta P \\ \Delta Q_1 \\ \Delta Q_2 \end{bmatrix} \tag{3}$$

where $_o$ refers to the starting values of all required variables, and the factor k has a value of 0.5 in the iterative process, with m representing the loop counter in Fig. 4.

2) Improved Sensitivity Matrix: The derivatives in the previous section were obtained assuming that the internal variables are isolated from the rest of the system, i.e. ignoring the power flow equations of the rest of the system, which under stressed conditions is not a valid assumption. Thus, since the maximum allowable values for V_X and V_Y are usually small (e.g. 0.05 p.u.), and these variables are quite sensitive to changes in the terminal voltages, using the technique presented in Section III-B1 may lead to convergence problems, especially when the system is stressed. Thus, G can be improved by using derivatives with respect to V_X and V_Y that considers voltage changes at the device terminals, since one can demonstrate that $dV_X \approx dV_1$ and $dV_Y \approx dV_2$; hence, in (1):

$$\frac{\partial P}{\partial V_X} = \alpha \frac{\partial P}{\partial V_1} \tag{4}$$

$$\frac{\partial P}{\partial V_Y} = \alpha \frac{\partial P}{\partial V_2} \tag{5}$$

and similarly for the corresponding Q_1 and Q_2 derivatives. In (4) and (5), α is a scalar (e.g. $\alpha = 0.5$) introduced to further reduce the step in the iterative procedure presented in Fig. 4, and thus improve convergence.

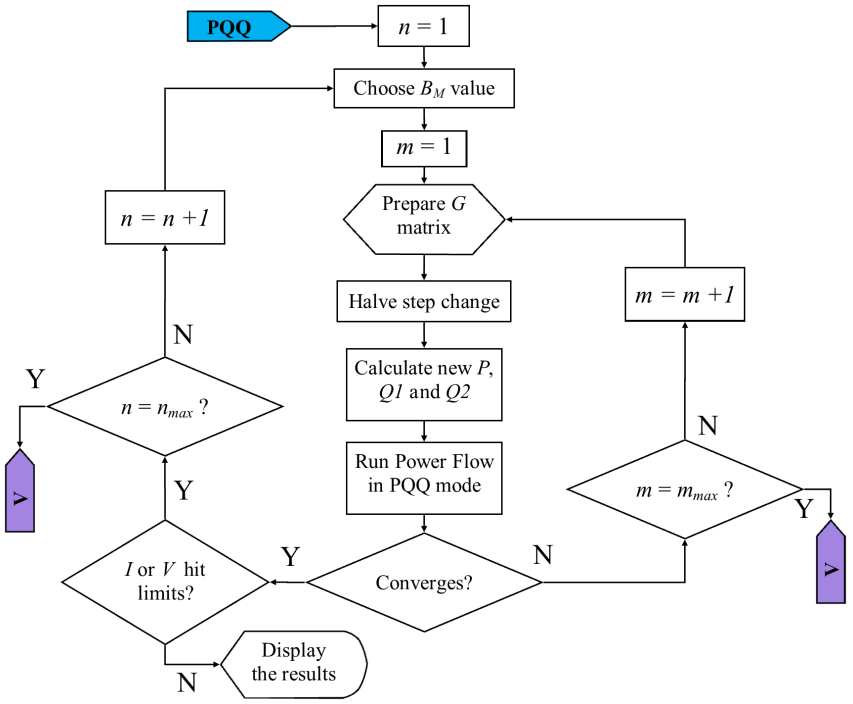

Fig. 4. Control strategy in PQQ mode.

3) Choosing B_M: The voltage magnitude on the inverters outputs depends on the shunt device voltage and thus the value of B_M; therefore, a "good" B_M value facilitates relieving the voltage limit violations. This is the first step depicted in Fig. 4 before the iterative procedure described in Section III-B1. The procedure to determine this value is explained next.

Based on the terminals voltages available from a previous power flow solution, an approximate working guess of V_M (and B_M) can be obtained as follows: Figure 5 depicts an exaggerated diagram of the voltage phasors, where the smallest values for V_X and V_Y are reached when $\boldsymbol{V}_M$ lies between $\boldsymbol{V}_{M1}$ and $\boldsymbol{V}_{M2}$. Therefore, to have $\boldsymbol{V}_M$ within this interval or close to it, first $\boldsymbol{V}_{M1}$ and/or $\boldsymbol{V}_{M2}$ are obtained using an initial guess for B_M to see if these yield feasible V_X and V_Y; if not, the interval between $\boldsymbol{V}_{M1}$ and $\boldsymbol{V}_{M2}$ is halved, with the resulting $\boldsymbol{V}_M$ yielding new $\boldsymbol{V}_X$ and/or $\boldsymbol{V}_Y$ phasors. If these $\boldsymbol{V}_X$ and/or $\boldsymbol{V}_Y$ are within their magnitude limits, then the associated value of B_M is computed; otherwise, the algorithm continues bisecting the interval until a feasible result, if it exists, is achieved, or a certain maximum iteration number (e.g. 3) is reached. The minimum $V_X + V_Y$ is used to choose whether to increase or decrease B_M, while halving the interval. The desired B_M value is calculated based on the obtained value for V_M; for discrete values of the shunt device, the closest step to the calculated value is chosen and used in the next step.

C. V Mode

In this mode, the two series voltage sources (see Fig. 2) are bypassed and $V_1 = V_2 = V_M$. The voltage magnitude at the terminals are regulated at a given level using the variable shunt susceptance B_M, with no active power flow control by the device. Thus, the power flow is run assuming the

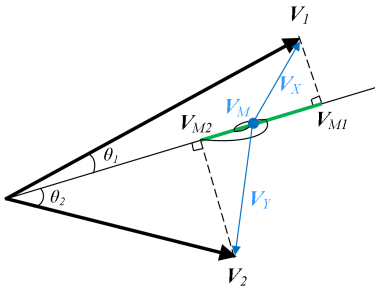

Fig. 5. Voltage phasor diagram.

device terminals and the shunt bus merged into one bus with a regulated voltage magnitude. If the power flow does not converge, the control mode switches to Z mode; otherwise, the largest of the input and the output currents (I_S and I_R) are checked with respect to the inverters' current limits; if it is within the limits, the device recovers and switches to PQQ mode, otherwise, based on the reactive power injection at the shunt bus obtained from the power flow analysis, the required B_M value is calculated. The shunt device has a maximum limit; thus, if the calculated B_M exceeds its maximum value, the shunt susceptance is fixed at B_{Mmax}, and the control mode is switched to Z mode. Otherwise, the control remains at V mode and final results are displayed. Note that if B_M is discrete, the voltage setpoint in the V mode will vary accordingly, i.e. is not a fixed value.

D. Z Mode

The Z mode corresponds to the HPFC at its minimum regulating capability. The B_M in this case is fixed at its

maximum value and $V_1 = V_2 = V_M$, and thus the device becomes a passive fixed shunt susceptance in the power flow analysis.

IV. OPF Model

The optimal power dispatch for a system can be calculated using an OPF formulation; the objective of this optimization problem is usually the maximization of social benefit or the minimization of production costs. System operational and security constraints as well as operating limits are usually included in an OPF formulation. Hence, mathematically the OPF can be stated as follows [8]:

$$\min_{P_G, Q_G, V, \delta} \quad Costs = \sum_{i \in \mathcal{G}} C_i\left(P_{Gi}\right) \tag{6a}$$

s.t.

$$P_{Gi} - P_{Di} = \sum_{j \in \mathcal{N}} V_i V_j (G_{ij}\cos(\delta_i - \delta_j) + B_{ij}\sin(\delta_i - \delta_j)) \qquad i \in \mathcal{N} \tag{6b}$$

$$Q_{Gi} - Q_{Di} = \sum_{j \in \mathcal{N}} V_i V_j (G_{ij}\sin(\delta_i - \delta_j) - B_{ij}\cos(\delta_i - \delta_j)) \qquad i \in \mathcal{N} \tag{6c}$$

$$P_{Gi\min} \le P_{Gi} \le P_{Gi\max} \qquad i \in \mathcal{G} \tag{6d}$$

$$Q_{Gi\min} \le Q_{Gi} \le Q_{Gi\max} \qquad i \in \mathcal{G} \tag{6e}$$

$$V_{i\min} \le V_i \le V_{i\max} \qquad i \in \mathcal{N} \tag{6f}$$

where $C_i(\cdot)$ stands for the generator i production cost, which is typically a quadratic function; $\mathcal{N}$ and $\mathcal{G}$ represent the set of all buses and generators, respectively; P_D and Q_D stand for the active and reactive demand which are assumed fixed here; P_G and Q_G represent the active and reactive powers of generators; G_{ij} and B_{ij} stand for line parameters; and V and δ correspond to the bus voltage phasor magnitudes and angles. Other operational or security constraints can be readily included as well (e.g. line flow limits), but were not considered here.

A lossless HPFC is considered here as part of the transmission system assets for dispatch purposes. In this context, the device can be represented in the OPF using the following power and circuit equations associated with Fig. 2:

$$P_1 = Re\left\{\boldsymbol{V}_1 \boldsymbol{I}_S^*\right\} \tag{7}$$

$$P_2 = Re\left\{\boldsymbol{V}_2 \boldsymbol{I}_R^*\right\} \tag{8}$$

$$P_1 = P_2 \tag{9}$$

$$\boldsymbol{V}_1 = \boldsymbol{V}_X + \boldsymbol{V}_M \tag{10}$$

$$\boldsymbol{V}_2 = \boldsymbol{V}_Y + \boldsymbol{V}_M \tag{11}$$

$$\boldsymbol{V}_M = \left(\frac{\boldsymbol{I}_S - \boldsymbol{I}_R}{jB_M}\right) \tag{12}$$

Proper ratings of the device imply a symmetrical loading on the series inverters, since both are assumed to share the load equally; this results in the following constraint:

$$|V_X - V_Y| \le \varepsilon \tag{13}$$

where ε is a small tolerance. Furthermore, the ratings of the converters and the shunt capacitor impose limits on the voltage magnitudes V_X and/or V_Y, and current magnitudes I_S and/or I_R, and B_M; these limits can be modeled through the following constraints:

$$0 \le V_X \le V_{Xmax} \tag{14}$$

$$0 \le V_Y \le V_{Ymax} \tag{15}$$

$$0 \le I_S \le I_{Smax} \tag{16}$$

$$0 \le I_R \le I_{Rmax} \tag{17}$$

$$0 \le B_M \le B_{Mmax} \tag{18}$$

Adding the HPFC equations and constraints (7)–(18) to (6) yields the full OPF model of the system including the HPFC for dispatch purposes. The solution of this optimization problem can be used to determine:

- The power dispatch of the system at minimum cost or maximum social benefit.
- The optimal setpoints of the HPFC control variables, including terminal voltage magnitudes and the device power flows.

In other words, the OPF solution yields an optimal power dispatch and the HPFC optimal control setpoints, corresponding to the lowest system operating costs for the assumed constraints. Also, this formulation, with proper large set of bounds for the HPFC constraints, can be used to determine optimal ratings of the device in design and planning studies for given system constraints, which is what the OPF model is used for in this paper.

V. Results and Discussions

The results of applying the discussed HPFC models to address congestion problems in a two-area benchmark test system and in Ontario-Canada's grid are presented in this section. In these studies, the power setpoints are varied and the voltage setpoints are chosen to be the same or very close to the values corresponding to the base-case conditions. This approach provides a meaningful and yet simple template to study and compare the power flow results without and with the added HPFC. The power flow and OPF studies of the two-area system are performed respectively, using PSAT, which is a MATLAB-based software package for power system analysis [9], and AMPL which is a mathematical modeling tool for optimization purposes [10]. The power flow and HPFC cost studies of the Ontario system are carried out using PSS®E [11].The detailed power flow model is integrated into the standard PSS®E solver using a custom Python code, which was used to introduce the mathematical model and procedure required to represent the HPFC within PSS®E [12].

A. Two-area Test System

A slightly modified version of Kundur's two-area test system is used for the analyses presented in this section [13].

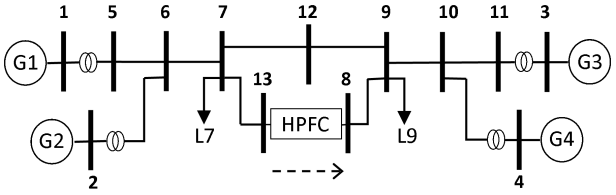

Fig. 6. Two-area test system.

TABLE I
TIE-LINE PARAMETERS (100 MVA, 230 KV BASE)

From	To	R [p.u.]	X [p.u.]	B [p.u.]
7	12	0.00733	0.0733	0.1925
12	9	0.00733	0.0733	0.09625
8	9	0.022	0.22	0.1925
7	13	0.022	0.22	0.09625

1) System Description: The system is loosely based on Ontario-Canada's network, representing the main generators, loads, and east-west system interconnections, which was developed to study small-disturbance oscillations. In this paper, the system is used to analyze congestion management issues associated with power flows over the tie-lines between the two areas, motivated by the actual congestion studies presented later for Ontario-Canada's grid. Figure 6 shows the single-line diagram of the system, and the original data can be found in [13]. The two areas are connected by a 220-km double-circuit tie-line. Both ends of the line are equipped with capacitor banks. In this study, the tie-line impedances as well as the reactive power demand/support at Buses 7 and 9 are slightly modified to force the system towards its limits; thus, the tie-line parameters are changed as per Table I, so that the overall tie-line impedance remains basically unchanged. The reactive power demands at Buses 7 and 9 are 300 MVAr and 50 MVAr capacitive, respectively.

The HPFC is connected between Bus 13 and Bus 8 in the lower corridor. The controller is assumed to start in PVV mode, thus defining setpoints for its active power flow and the voltage magnitudes at its terminals, which can be set arbitrarily as desired by the operator or based on a chosen dispatch policy. The setpoints are chosen here so that the flows and voltages are consistent with the base system without HPFC at base load for comparison purposes; however, the setpoints can be chosen optimally for different operating points using the proposed OPF model.

2) Power Flow Results: The loadability studies performed on the system assume Buses 9 and 2 as power sink and source, respectively. Thus, the power transfer between these two nodes is increased until the power flow cannot be solved, gradually increasing the load in 0.1 p.u. steps. The required HPFC parameters used here are the following:

- Maximum current magnitudes (I_S and I_R): 2 p.u.
- Maximum voltage magnitude for the converters including transformers (V_X and V_Y): 0.04 p.u. (9.2 kV).
- Discrete shunt susceptance with four equal steps (0.2 p.u. each): $0 \leq B_M \leq 0.8$ p.u. The size of this capacitor can be considered reasonable compared to the existing capacitors at Buses 7 and 9.
- Active power share of the lower corridor with respect to the total tie-line flow: 25%.
- Voltage magnitude setpoint at the terminals: 0.9557 p.u.

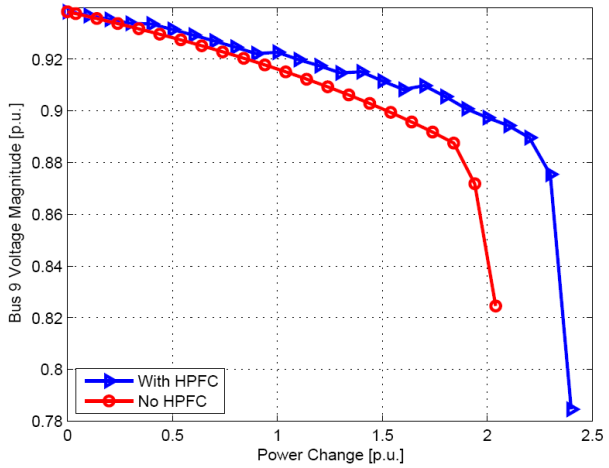

Fig. 7. PV curves at Bus 9 with and without HPFC.

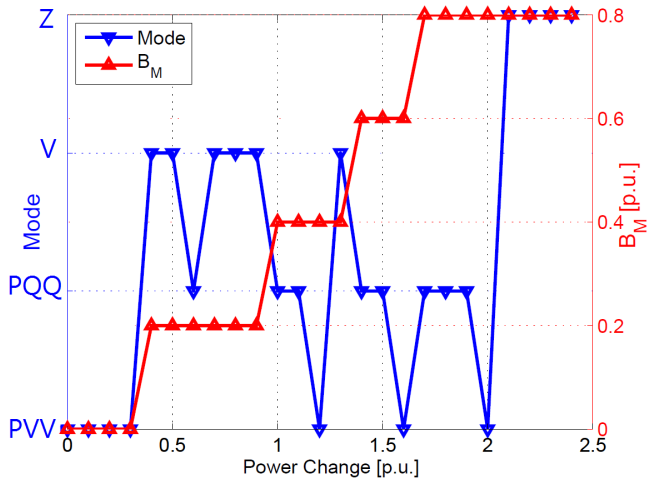

Fig. 8. HPFC control modes and B_M as the loading level increases.

The maximum loadability of the system at Bus 9 increases from 204 MW to 240 MW when introducing the HPFC. The voltage profile at the sink-bus Bus 9 is depicted in Fig. 7, with and without the HPFC; observe that the HPFC improves the maximum loadability and voltage profile.

The HPFC control modes and B_M values at different operating points are shown in Fig. 8. Note that the device starts in the PVV mode and switches to different modes according to the system requirements at different operating points as the load increases. At the last four operating points, the HPFC has exhausted its capability limits, and thus behaves as a fixed shunt susceptance in the Z mode. Observe that the algorithm transitions to the best feasible mode using the available shunt susceptance steps, based on the procedure depicted in Fig. 4.

3) OPF Results: The optimal voltage ratings of the controller can be chosen using the proposed OPF formation

TABLE II
GENERATOR COST $C(P_G) = a + bP_G + cP_G^2$.

Bus No.	a [$/h]	b [$/MWh]	c [$/MW^{2}h]	P_{Gmax} [MW]
1	800	20	0.002	2000
2	800	20	0.002	2000
3	1600	40	0.004	2000
4	1600	40	0.004	700

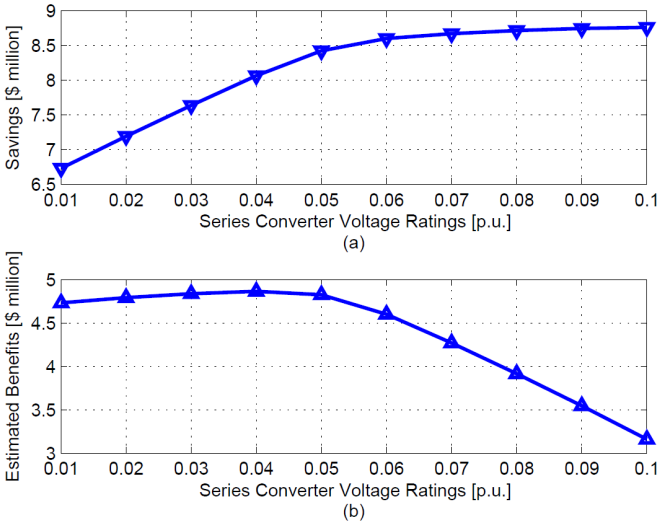

Fig. 9. Economic analysis for different voltage ratings: (a) Savings, and (b) Cost-benefit.

assuming the rest of the parameters remain as defined earlier, since current ratings mostly depend on the expected maximum power flow, and the shunt component is assumed to be known. The generators in the area to the right, i.e. Buses 3 and 4 which are closer to the demand centre, are assumed to be more expensive than the generators in the left area (Buses 1 and 2), as illustrated in the generator dispatch cost data in Table II. This uneven pricing allows to study the financial impact of the tie-line transfer capability, to be relieved by the introduction of the HPFC. The unit cost of HPFC converters including required installation/constructions is assumed to be $100,000/MVA; this figure for the capacitor banks is close to $20,000/MVAr [14], [15].

The expected annual operation savings due to the device installation shown in Fig. 9(a) can be calculated using a typical load duration curve [16]. Note the savings increase as the voltage ratings increase, as expected. One can compare the effect of different voltage ratings by subtracting the installation costs from the savings, resulting in the cost benefit curve depicted in Fig. 9(b) which has a maximum at a 0.04 p.u. voltage rating.

B. Application to Ontario-Canada's Grid

A detailed model of the Ontario-Canada system is used here to examine the use of the HPFC model within a realistically large system, motivated by the interest in and relevance of these studies to several entities associated with the provincial electricity grid. The prospective HPFC installation would provide system operators with the ability to control the flows and adequately regulate the voltage profile in the grid, thus providing congestion relief at peak-demand and voltage support in the case of contingencies. Therefore, the performance of the HPFC under realistic conditions and scenarios are studied here, and the results are presented and discussed next.

1) Network Model: The base-case dataset for the grid was obtained from Ontario-Canada's Independent Electricity System Operator (IESO), and contains information for a power flow solution at a peak demand period [17]. It spans the power network from New Brunswick to Kentucky, including Ontario, New York, and areas in between. It has 6895 buses, 38085 branches, 1890 generator units, and a total load of 267 GW.

2) Potential HPFC Locations: Based on the input from the IESO, the following four locations on the Ontario grid were studied for the potential HPFC installation, given that the associated lines are prone to congestion problems, as determined based on PV-curves and related studies performed for different loading scenarios:

a) A 115 kV double-circuit in the Ottawa region.
b) A 115 kV double-circuit in Bell River.
c) A 115 kV double-circuit in the Burlington area.
d) Two 220 kV double-circuits around Trafalgar supplying Toronto, the main load center of the province.

The approximate locations are marked on the provincial grid map shown in Fig. 10 [18]. All of these locations have parallel circuits that allow to analyze the power flow regulation capabilities of the HPFC.

Each of the four suggested locations was studied with a hypothetical HPFC installation, and the impact of relevant contingencies (trip of one of the parallel circuits) was investigated. All of these locations are suitable for the installation of the HPFC and would benefit from its addition. However, only the results pertaining to Location d are presented here, since the loading of this circuit is significantly greater (and closer to its limits) compared to the other locations; thus, the impact of the controller can be better examined under normal and contingency conditions. Furthermore, the circuit associated with this location is a crucial link in the grid supplying the main load center of the province, and future demand increases would further stress this interconnection. Hence, the presented studies for this location are of significant interest and relevance.

3) Power Flow Results: The double-circuit at Location d connects Trafalgar to Richview, a suburb of Toronto, with each of the parallel circuits carrying roughly 270 MW in the base case. Hence, the HPFC is assumed to be installed on one of the circuits (Line 1), thus controlling its flow directly and the flow of the parallel circuit (Line 2) indirectly. The voltage magnitudes at the controller terminals are assumed to be regulated around a given setpoint, since the controller is considered to start in PVV mode. The basic HPFC parameters used here are the following (100 MVA, 220 kV base):

- Maximum current magnitudes (I_S and I_R): 5 p.u.
- Maximum voltage magnitude for the converters including transformers (V_X and V_Y): 0.05 p.u.

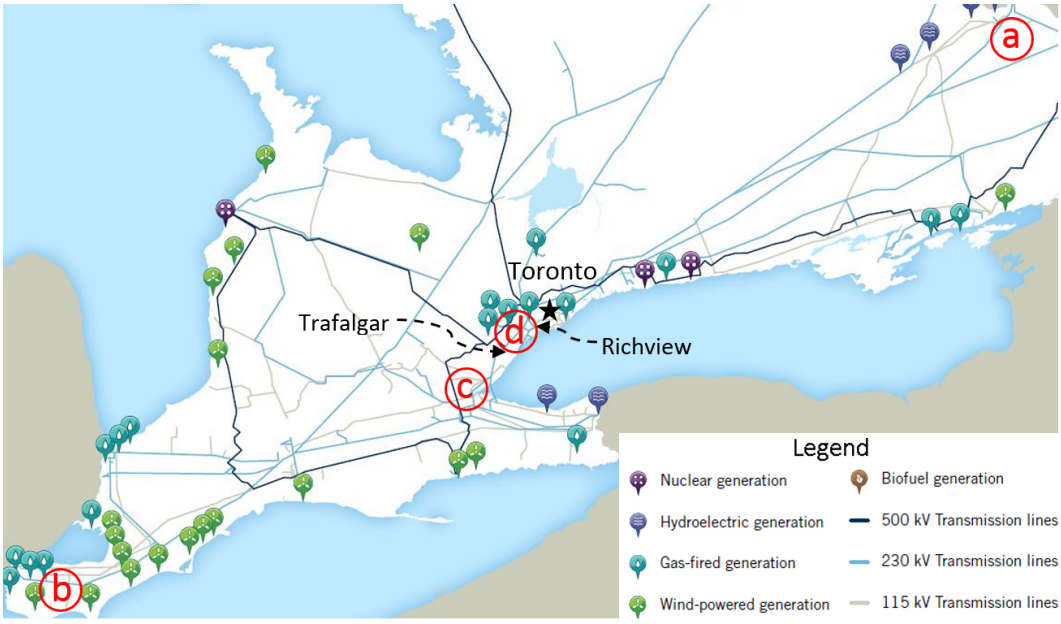

Fig. 10. Ontario map and potential installation locations of the HPFC [18].

- SVC-based shunt susceptance: $0 \leq B_M \leq 1.5$ p.u.
- Range of active-power control in Line 1 with respect to the base case (maximum line rating of 719 MW): 20%–260% (54 MW–700 MW).
- Voltage magnitude setpoint at the terminals (slightly higher than the base-case value of 1.109 p.u.): 1.119 p.u. Note that the voltage magnitudes for the base-case in the Ontario grid correspond to the actual system values provided by the IESO.

To study the impact of the HPFC at the chosen location, the active-power setpoint is gradually increased from 54 MW to 700 MW, while the rest of the system remains intact. Note that this study is different from what was presented in Section V-A, since the load/generation is not altered, with the HPFC regulating flows and voltage magnitudes according to given setpoints. Figure 11 shows the active powers flowing through Lines 1 and 2 as the controller setpoints change until it reaches its capability limits and switches to PQQ mode; this figure highlights the direct and indirect controls over the flows through parallel circuits using the controller. Figure 12 shows B_M and the HPFC control modes highlighting the transition between PVV and PQQ modes. The descending B_M values in PVV mode indicate the increasing need for reactive power at the sending end (Trafalgar) as the active power flow increases. The voltage magnitudes at Trafalgar and Richview remained fixed at their initial values, indicating a stiff system at the lines' terminals. The change in the active power losses in the Ontario system with the HPFC and different controller setpoints with respect to the base case is illustrated in Fig. 13. Note that the impact on the system losses is not considerable, due to the stiff nature of the Ontario grid, the sizing of the controller, and the fact that the setpoints chosen for the HPFC approximately match the base-case values.

Figures 11 and 12 show the powers, control modes, and

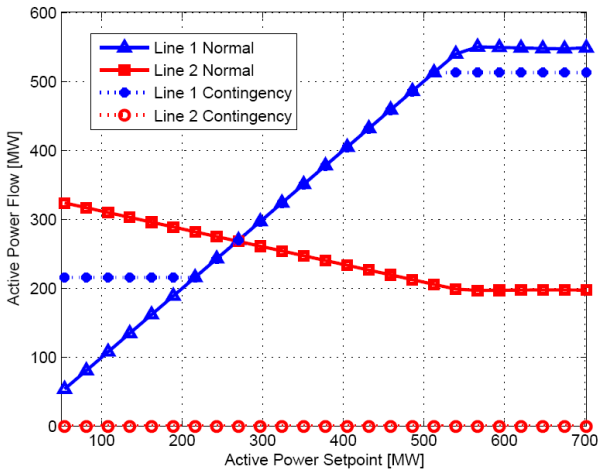

Fig. 11. Active power flow in the parallel circuits at Ontario's Location d.

B_M values for the controller when Line 2 is tripped, i.e. under contingency conditions. Observe that the controller reaches its limits and changes control modes at lower transfer rates, with the maximum power transfer level saturating at a lower value.

4) Cost Analysis: A basic comparison between the capital-cost requirements of different configuations of the HPFC is presented here. For this comparison, it is considered that an HPFC can be realized using two VSCs, plus an SVC, a switched capacitor, or an STATCOM. A full cost-benefit study was not possible in this case, as the generators' costs were not available, since this is considered sensitive market information by the IESO; hence, the proposed OPF model to optimally size the HPFC could not be applied in this particular study.

The hardware and installation costs are extracted from [14], [15], and [19]. Based on the results obtained previously for

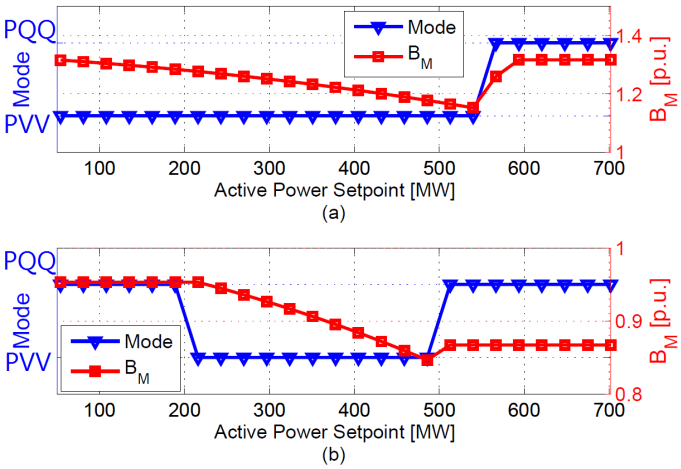

Fig. 12. HPFC control modes and B_M as the loading level increases under: (a) normal, and (b) contingency conditions.

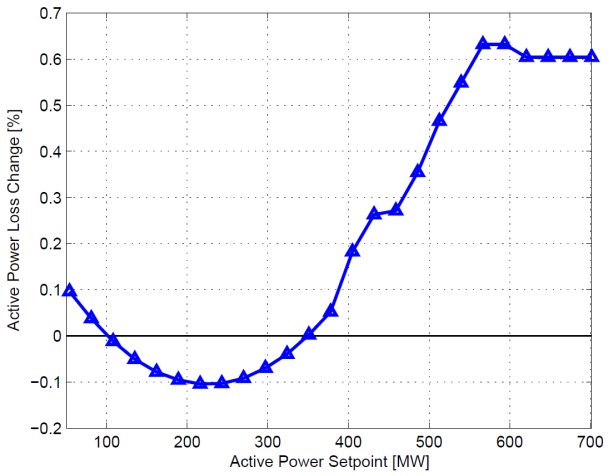

Fig. 13. Change in active power loss in the system with the HPFC with respect to the base case.

different desired control ranges, under normal conditions, one can obtain the controller ratings; thus, for example, for a 400 MW power transfer limit, the converter current ratings would be approximately 3.75 p.u., whereas the voltage ratings would correspond to 0.022 p.u., and B_M would be 1.21 p.u. from Fig. 12. Figure 14 shows the capital cost requirements with respect to the power ratings for the HPFC with different configurations for its shunt component, namely, an SVC with an 80 MVAr fixed capacitor, an equivalent switched capacitor bank, and an equivalent STATCOM; observe the significant cost advantages of the HPFC with shunt capacitor banks or SVC.

VI. Conclusions

Steady-state models of the HPFC for power flow and optimal power flow studies have been proposed in this paper, considering the device's various control modes. A strategy for handling the violated constraints in power flow calculations has been considered, and an optimal dispatch of the device in

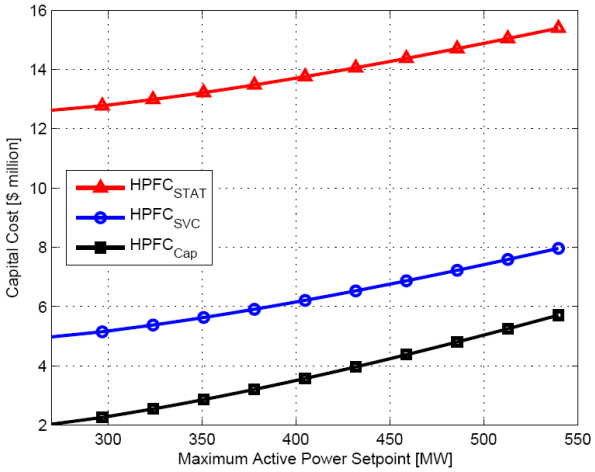

Fig. 14. Capital costs of the HPFC with different shunt components for different control ranges.

the system was examined within an OPF context, considering relevant operational constraints, to determine its optimal size and setpoints. The models were validated and tested using a two-area benchmark test system, and their practical application and advantages were demonstrated in Ontario-Canada's grid. From the presented studies, it can be concluded that the HPFC is an attractive option for congestion relief in real power networks.

Acknowledgments

The authors would like to thank Dr. Jovan Bebić of GE Energy Consulting, USA, for his insightful comments and suggestions, and the IESO for their valuable input.

References

[1] X. P. Zhang, C. Rehtanz, and B. Pal, *Flexible ac Transmission Systems, Modelling and Control*. Berlin, Germany: Springer 2006.
[2] I. Axente, R. K. Varma, and W. Litzenberger, "Bibliography of FACTS: 2000 – part I IEEE working group report," in *Proc. IEEE PES General Meeting*, pp. 1–6, 2011.
[3] S. Arabi, P. Kundur, and R. Adapa, "Innovative techniques in modeling UPFC for power system analysis," *IEEE Trans. Power Syst.*, vol. 15, no. 1, pp. 336-341, Feb. 2000.
[4] S. Zelingher, B. Fardanesh, B. Shperling, S. Dave, L. Kovalsky, C. Schauder, and A. Edris, "Convertible Static Compensator project - hardware overview," in *Proc. IEEE PES Winter Meeting*, vol. 4, pp. 2511–2517, 2000.
[5] J. Z. Bebic, P. W. Lehn, and M. R. Iravani, "The Hybrid Power Flow Controller - a new concept for flexible ac transmission," in *Proc. IEEE PES General Meeting*, Montreal, Quebec, Canada, pp. 1–8, 2006.
[6] V. K. Sood and S. D. Sivadas, "Simulation of Hybrid Power Flow Controller," in *Proc. Int. Conf. Power Electronics, Drives and Energy Systems (PEDES) & Power India*, pp. 1–5, Dec. 2010.
[7] N. R. Merritt and D. Chatterjee, "Performance improvement of power systems using Hybrid Power Flow Controller," in *Proc. Int. Conf. Power and Energy Systems (ICPS)*, pp. 1–6, Dec. 2011.
[8] A. G. Expósito, A. J. Conejo, and C. Cañizares, *Electric Energy Systems, Analysis and Operation*. Boca Raton, FL., USA: CRC Press, 2009.
[9] F. Milano, "An open source power system analysis toolbox," *IEEE Trans. Power Syst.*, Vol. 20, No. 3, pp. 1199-1206, Aug. 2005.
[10] R. Fourer, D. Gay, and B. Kernighan, *AMPL: A Modeling Language for Mathematical Programming*. Pacific Grove, CA., USA: McGraw-Hill, 2003.
[11] PSS®E 33, Program Application Guide, 2013.

[12] Python, Program Website, [Online]. Available: https://www.python.org/
[13] P. Kundur, *Power System Stability and Control*. New York: McGraw-Hill, 1994.
[14] M. Eslami, H. Shareef, A. Mohamed, and M. Khajehzadeh, "A survey on Flexible AC Transmission Systems (FACTS)," *Przeglad Elektrotechniczny*, Issue 01a, pp. 1–11, Jan. 2012.
[15] "Flexible AC Transmission Systems benefits study," San Diego Gas and Electric, San Deigo, CA., USA, Oct. 1999.
[16] "18-month outlook," Ontario Independent Electricity System Operator (IESO), Public report, May 2010 [Online]. Available: http://www.ieso.ca
[17] Ontario Independent Electricity System Operator (IESO), [Online]. Available: http://www.ieso.ca
[18] Ontario Energy Report [Online]. Available: http://www.ontarioenergyreport.ca/
[19] R. M. Mathur and R. K. Varma, *Thyristor-based FACTS Controllers for Electrical Transmission Systems*. New York: John Wiley & Sons, 2002.

Behnam Tamimi (S05) received the B.Sc. degree in Electronics Engineering from the University of Tehran, Tehran, Iran, in 2001 and the M.Sc. degree in electrical engineering from KNT University, Tehran, in 2003. He is currently a PhD student at the University of Waterloo, Canada. He has been a member of two IEEE-PES taskforces on benchmarking test systems for stability analysis. His research interests include power system analysis in the context of liberalized markets, and power electronics applications in power systems.

Claudio Cañizares (S86, M91, SM00, F07) is a Professor at the University of Waterloo since 1993 and currently serves as the Hydro One Endowed Chair and the Associate Chair for Research of the ECE Department. His highly cited research activities focus on the study of modeling, simulation, computation, stability, control, and optimization issues in power and energy systems in the context of competitive energy markets and smart grids. He is a Fellow of the IEEE, of the Royal Society of Canada, and of the Canadian Academy of Engineering, and the recipient of the 2016 IEEE Canada Electric Power Medal and of other various awards and recognitions from IEEE-PES Technical Committees and Working Groups, where he has held several leadership positions.

Claudia Battistelli (M08) received her MS (2006) and PhD (2010) degrees in Electrical Engineering from the Federico II University of Naples, Italy. She was at the Electrical and Computer Engineering Department of the University of Waterloo, Canada, as a visiting PhD student in May 2008-Apr. 2009, and as a Postdoctoral Fellow in Jan.-Dec. 2013. Since Jan. 2014, she works as a Research Associate at the Electrical and Electronic Engineering Department of Imperial College, London, UK. Her research areas include mathematical optimization techniques, power systems analysis, and sustainable power and energy systems in the Smart Grid context.